Previous heat treatment inducing different plasma nitriding behaviors in martensitic stainless steels

C. A. Figueroa, F. Alvarez, D. R. G. Mitchell, G. A. Collins, and K. T. Short

---

Articles you may be interested in

Plasma nitriding process by direct current glow discharge at low temperature increasing the thermal diffusivity of AISI 304 stainless steel
J. Appl. Phys. **113**, 063507 (2013); 10.1063/1.4790631

Influence of the microstructure on steel hardening in pulsed plasma nitriding
J. Vac. Sci. Technol. A **26**, 328 (2008); 10.1116/1.2889395

Structural modifications and corrosion behavior of martensitic stainless steel nitrided by plasma immersion ion implantation
J. Vac. Sci. Technol. A **23**, 693 (2005); 10.1116/1.1931681

Anisotropic strain in nitrided austenitic stainless steel
J. Appl. Phys. **88**, 3323 (2000); 10.1063/1.1289520

Microstructure and corrosion resistance of plasma source ion nitrided austenitic stainless steel
J. Vac. Sci. Technol. A **15**, 421 (1997); 10.1116/1.580501

Previous heat treatment inducing different plasma nitriding behaviors in martensitic stainless steels

C. A. Figueroa[a)]
Australian Nuclear Science and Technology Organisation, Private Mail Bag 1, Menai, New South Wales 2234, Australia and Instituto de Física "Gleb Wataghin," Unicamp, Campinas, São Paulo 13083-970, Brazil

F. Alvarez
Instituto de Física "Gleb Wataghin," Unicamp, Campinas, São Paulo 13083-970, Brazil

D. R. G. Mitchell, G. A. Collins, and K. T. Short
Australian Nuclear Science and Technology Organisation, Private Mail ag 1, Menai, New South Wales 2234, Australia

In this work we report a study of the induced changes in structure and corrosion behavior of martensitic stainless steels nitrided by plasma immersion ion implantation (PI^3) at different previous heat treatments. The samples were characterized by x-ray diffraction and glancing angle x-ray diffraction, scanning electron microscopy, energy dispersive x-ray spectroscopy, and potentiodynamic measurements. Depending on the proportion of retained austenite in the unimplanted material, different phase transformations are obtained at lower and intermediate temperatures of nitrogen implantation. At higher temperatures, the great mobility of the chromium yields CrN segregations like spots in random distribution, and the α'-martensite is degraded to α-Fe (ferrite). The nitrided layer thickness follows a fairly linear relationship with the temperature and a parabolic law with the process time. The corrosion resistance depends strongly on chromium segregation from the martensitic matrix, as a result of the formation of CrN during the nitrogen implantation process and the formation of Cr_xC during the heat treatment process. Briefly speaking, the best results are obtained using low tempering temperature and low implantation temperature (below 375°) due to the increment of the corrosion resistance and nitrogen dissolution in the structure with not too high diffusion depths (about $5-10$ μm). © *2006 American Vacuum Society.* [DOI: 10.1116/1.2219759]

I. INTRODUCTION

Plasma nitriding of metal alloys is a widespread thermochemical technique of surface modification for further improvement of mechanical properties such as wear, hardness, fatigue, as well as chemical properties such as corrosion resistance and biocompability.[1,2] Many works in the last three decades were focused on the development of diverse technologies in plasma nitriding and the study of the influence of the nitrogen implantation in different types of steels.[3,4] However, there is no clear approach with respect to the influence of the heat treatment in the global process. Quenching and tempering processes can profoundly modify the nanostructure and phases present in the same steel before performing a plasma nitriding treatment.[5] Moreover, materials such as martensitic stainless steels (MSSs) are very susceptible to their previous history because they are metastable alloys obtained by fast cooling where structural modifications are driven without diffusion. Depending on tempering temperature and time, a more or less retained austenite is presented in the martensitic structure.

It is well known that stainless steels have a very stable oxide layer (Cr_2O_3) on the surface, given the corrosion resistance, but create a potential barrier for nitrogen implantation.[6–9] In order to improve the nitrogen chemical potential for further nitrogen diffusion, plasma immersion ion implantation (PI^3) becomes a suitable technique because the high voltage applied produces an energetic ion bombardment, thus augmenting the nitrogen retention.[10–13] Furthermore, plasma nitriding of austenitic stainless steels is a model system where PI^3 demonstrated the efficiency of decreasing the surface potential barrier compared to rf plasma.[14]

Finally, pathways for plasma surface engineering can be opened, bearing in mind not only the type of steel and the process variables, but also the previous heat treatment of the base material.

In this article we report the influence of the previous heat treatment and the implantation temperature and time on plasma nitriding of MSS by PI^3. The aim of the study is to investigate the phase transformation, morphology, diffusion properties, and corrosion resistance of the commercial MSS AISI 420 after nitrogen incorporation at different temperatures, process times, and heat treatments. Depending on the previous heat treatment, different phases are obtained at lower and intermediate temperatures. At higher temperatures, the relatively great mobility of the nitrogen and chromium in the matrix produces a substantial precipitation of CrN, trans-

---

TABLE I. Summary of the treatment conditions of AISI 420 by PI^3. Nitrogen gas pressure was 15 μbars; high voltage (HV) pulse length was 100 μs; pulse duty cycle was adjusted to maintain a constant dose rate.

Previous heat treatment conditions	Temperature (°C)	Process time (h)	HV bias voltage (keV)	Dose rate (10^{14} ions cm^{-2} s^{-1})
A: Hardened at 1040 °C for 1 h, cold quenched. Tempered at 310 °C for 1 h.	340–475	9	30	1
B: Hardened at 1040 °C for 1 h, cold quenched. Tempered at 530 °C for 1 h.	360–500	1, 4, and 9	5–25	0.5–2.5

forming the original α'-martensite phase in α-Fe (ferrite). The nitrided layer thickness follows a fairly linear relationship with temperature and a parabolic law with process time. The corrosion resistance is degraded by an increase in nitriding temperature, showing an interval where there is an abrupt precipitation of CrN. This process starts with segregations at the grain boundaries and then, at higher temperatures, in different places of the matrix. A lower tempered temperature improves the corrosion resistance, avoiding intergranular sensitization by Cr$_x$C formation.

The article is organized as follows. In Sec. II, the experimental conditions used are introduced, stressing the techniques employed in the study. In Sec. III, the results are presented and discussed, focusing on the phase transformation by nitrogen implantation depending on the previous heat treatment. Finally, in Sec. IV the conclusions are presented.

II. EXPERIMENT

The study is based on martensitic stainless steel AISI 420 (C: 0.3, Si: <1.0, P: <0.04, S: <0.03, Mn: <1.0, Ni <1.0, Cr: 13.0, and Fe: balance). Several disks ~25 mm in diameter and ~3 mm thick were cut from a bar stock and then ground and polished to a 1 μm size diamond abrasive powder finish. These samples were processed using the PI^3 system described elsewhere (ANSTO).[15] Two sets of samples were prepared at different previous heat treatments (HT A and B). Table I shows a summary of the treatment conditions.[16] As experimentally corroborated, the variations in temperature and process time are more important than ion energy, implantation dose, and nitrogen partial pressure in the chamber. Indeed, these parameters determine the material phase transformations, morphology, and corrosion behavior reported in this article.

The phase evolution was studied by x-ray diffraction (XRD) using a Siemens D500 x-ray diffractometer and the Co $K\alpha$ radiation line in glancing angle (GA) (and a mean x-ray depth penetration of ~1 μm) and in the conventional Bragg-Brentano (BB) (and a mean x-ray depth penetration of ~4 μm) geometry. The surface morphology of the as-nitrided layers was observed by scanning electron microscopy (SEM) using secondary electron images (SEI) and backscattered electron images (BEI) in a JEOL JSM-6400. Standard metallographic cross sections were prepared and etched with Marble's solution (10 g copper sulfate in 100 ml

of 6M hydrochloric acid) to reveal the microstructure of the nitrided layers. In order to determine chemical composition, samples were analyzed by energy dispersive x-ray spectroscopy (EDS) in the SEM.

Finally, the corrosion behavior of the nitrided samples was studied by electrochemical methods. 1 cm^2 pieces of the samples were embedded in bakelite resin so that only the nitrided surface was exposed, and an insulated electrical connection was made to the rear of the sample. Measurements were performed with a VoltaLab PGZ 402 using a conventional three-electrode cell. A solution of 3% NaCl was made from analytical grade reagent and de-ionized water (18.2 MΩ). The auxiliary electrode was a Pt wire, and all voltages were measured against a Ag/AgCl (1M) reference electrode. The potentiostatic anodic polarization curves were obtained at a potential scan rate of 1 mV s^{-1}.

III. RESULTS AND DISCUSSION

Figures 1(a) and 1(b) show the x-ray diffraction pattern of implanted samples at variable temperature, using a base material with HT A and B, respectively. First, it is important to remark that the HT A yields a higher proportion of retained austenite than HT B in the untreated material. Second, different behaviors are obtained up to 475 °C (higher temperatures) where both implanted materials show similar diffraction patterns. Nitrogen implantation and its posterior thermal diffusion in iron alloys produce phase transformations in depth. According to Figs. 1(a) and 1(b), the heat treatment conditions are fundamental in these transformations, where a higher content in retained austenite in the base material yields different phases at lower and intermediate temperatures. Table II shows a summary of the phases involved in implanted samples at different temperatures and heat treatments.

In order to study the phase transformation mechanism, glancing angle x-ray diffraction (GAXRD) patterns were taken. Figures 2(a) and 2(b) show the glancing angle (5°) and conventional XRD patterns of implanted samples at 340 °C (HT A) and 360 °C (HT B), respectively (lower temperatures). Both HT yield ε-(Fe,Cr)$_3$N, but the sample at HT A also shows γ_N phase in the GAXRD. Moreover, the γ phase becomes important and more γ_N phase is present in depth [BB geometry, see Fig. 2(a)]. It is important to remark that the proportion of fcc phases (γ_N and γ) is higher than the
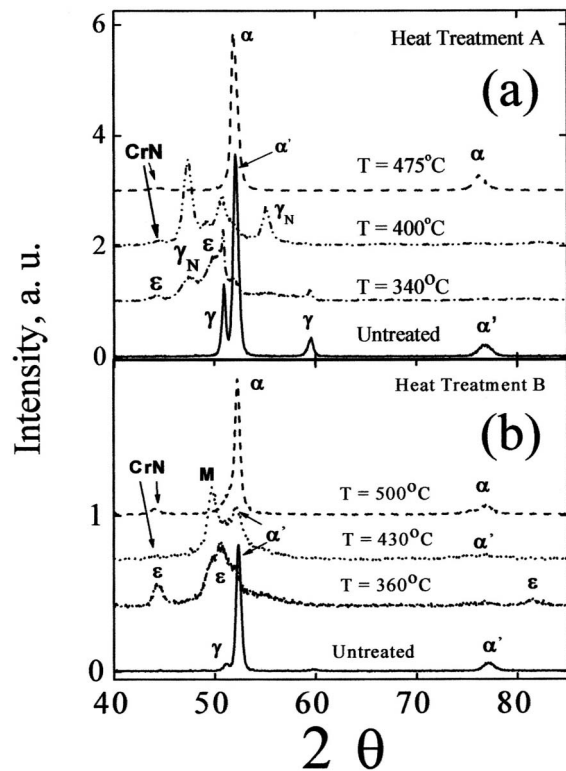
FIG. 1. [(a) and (b)] Evolution of the x-ray diffraction patterns as a function of temperature using previous HT A and B, respectively. The process time was fixed at 9 h.
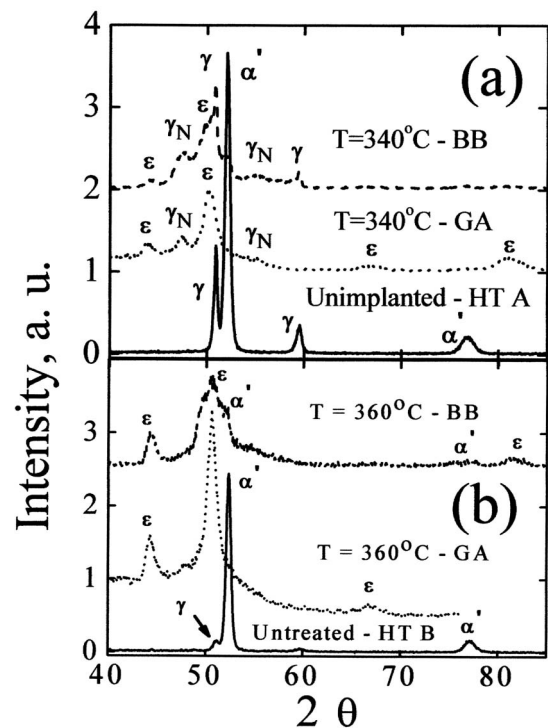

FIG. 2. [(a) and (b)] Comparison of x-ray diffraction patterns in glancing angle and conventional geometry at lower implantation temperatures using previous HT A and B, respectively. The process time was fixed at 9 h.

retained austenite in the base material. On the other hand, Fig. 2(b) shows mostly the formation of ε-(Fe,Cr)$_3$N. At intermediate temperatures, higher nitrogen diffusion avoids major formation of nitrogen rich phases as ε-(Fe,Cr)$_3$N. Figures 3(a) and 3(b) show glancing angle (5°) and conventional XRD patterns of implanted samples at 400 °C (HT A) and 430 °C (HT B), respectively. Figure 3(a) shows a clear phase transformation to γ_N (major phase) and ε-(Fe,Cr)$_3$N. This higher content of retained austenite in HT A induces a way for further creation of fcc-like structures from the α-martensite. Yu *et al.* have observed this type of transformation in AISI 304 where, by mechanical polishing, a surface structure quite similar with our HT A base material was obtained.[17] On the other hand, Fig. 3(b) shows qualitative differences when the HT B base material is nitrided. The ε-(Fe,Cr)$_3$N obtained at 360 °C [see Fig. 2(b)] disappears, and a possible interpretation for the α-martensite transformation is the "expanded martensite" [peak M in Fig. 3(b)] with

little CrN formation. Kim *et al.*[18] have proposed the existence of the M phase, and Muñoz-Páez *et al.*[19] have shown that the presence of elements such as chromium, vanadium, and other transition metals, can stabilize a supersaturate α phase, avoiding the transformation to γ_N. These different behaviors in phase transformations, depending on the previous heat treatment, are consistent with the presence of more or less retained austenite in the martensitic matrix.

At higher temperatures, the chromium has a great mobility, segregating from the martensitic matrix and precipitating mostly as CrN. Figure 4 shows similar behaviors of samples nitrided at 475 °C (HT A) and 500 °C (HT B). The α'-martensitic phase is degraded to α-Fe (ferrite) and CrN.[5]

A surface and cross-section analysis by SEM and EDS of these samples was performed to explore the surface morphology, compound segregations, and the nitrided layer thickness as functions of nitriding temperature and process time. Figures 5(a)–5(e) show the evolution of the "as implanted" surface morphology using the SEI mode of samples with HT A

TABLE II. Phase composition of implanted samples in both HT at different temperatures and fixed process time of 9 h.

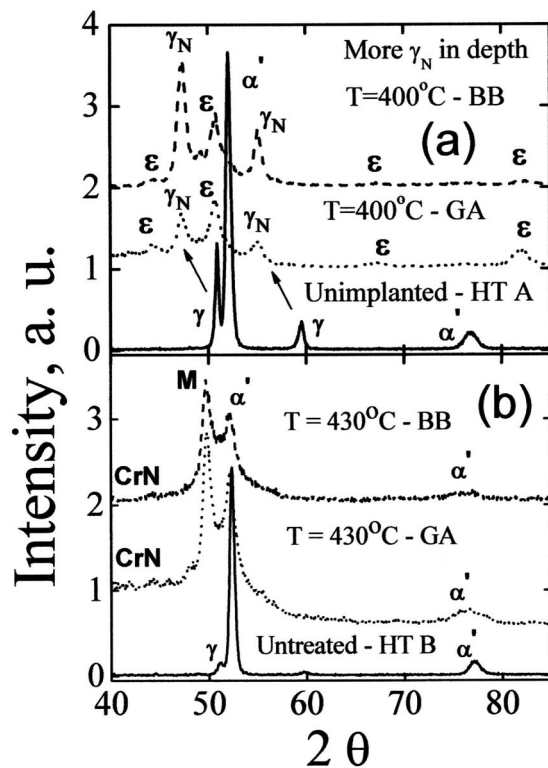| Heat treatment	Unimplanted	Low temperature (°C)	Intermediate temperature (°C)	High temperature (°C)
A	α', γ	ε, γ_N, γ at 340 °C	ε, γ_N at 400 °C	α, CrN at 475 °C
B	α', γ (little)	ε, α' at 360 °C	M, α', CrN (little) at 430 °C	α, CrN at 500 °C

FIG. 3. [(a) and (b)] Comparison of x-ray diffraction patterns in glancing angle and conventional geometry at intermediate implantation temperatures using previous HT A and B, respectively. The process time was fixed at 9 h.

FIG. 5. [(a)–(e)] Evolution of secondary electron images (SEI mode) of the surface of implanted samples as a function of temperature. The matrix and grain boundaries are indicated.

at variable temperature and fixed time of 9 h. At the lowest temperature, well defined grain boundaries are identified. Following the photos, the higher the temperature, the lower the border definition between grains. At the highest temperature, undefined grain boundaries are observed. Moreover, the quantity and size of little spots at the grain boundaries are increased with the implantation temperature.

Figures 6(a)–6(e) show the evolution of the as implanted surface composition and compound segregations using the
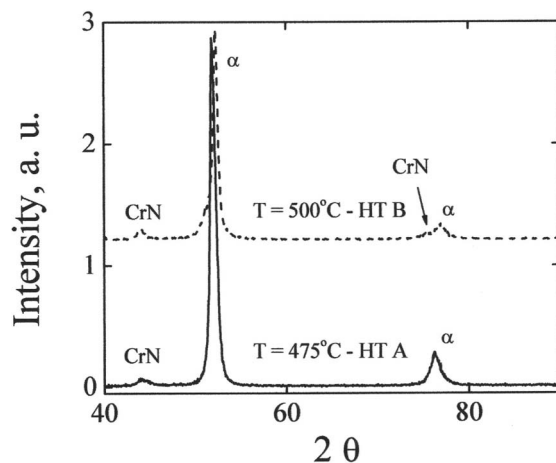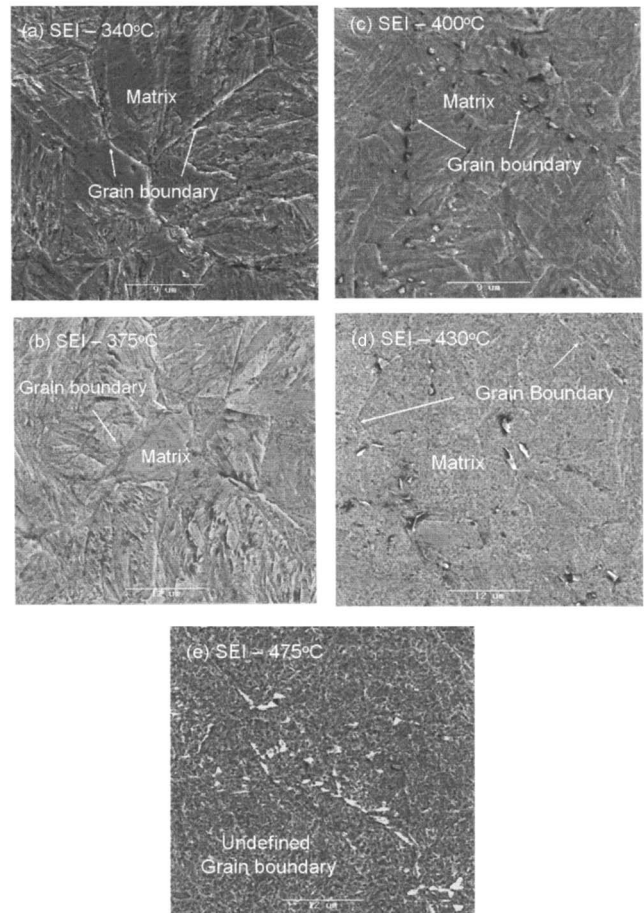

FIG. 4. Comparison of x-ray diffraction patterns at higher implantation temperatures using previous HT A and B. The process time was fixed at 9 h.

BEI mode of samples with HT A at variable temperature and fixed time of 9 h. For comparison purposes, these photos show the same region as the ones in Fig. 5(a)–5(e). The backscattering photos were obtained in the composition mode where a darker tonality means a higher concentration of light elements.[20] In order to compare the chromium content in the matrix and the one precipitated at the grain boundary, EDS measurements were performed. At the lowest temperature, the grain boundaries present a dark tonality where the chromium content is similar to that in the matrix. Figure 6(b) shows the beginning of the chromium segregation process, and a few dark spots (with high chromium content) can be observed at grain boundary.[21] The higher nitrogen concentration and density of dislocations located at the grain boundary act as preferential nucleating sites.[22,23] This process becomes very important and, at intermediate temperatures, more and bigger spots are present. At higher temperatures, the segregations of CrN follow a random distribution where the grain boundaries are not quite visible. Corroborating the XRD observations, the diffusion coefficient of chromium is improved with the temperature, and the random distribution of CrN segregations is in agreement with the α'-martensite degradation to α-Fe (ferrite). The surface morphology be-
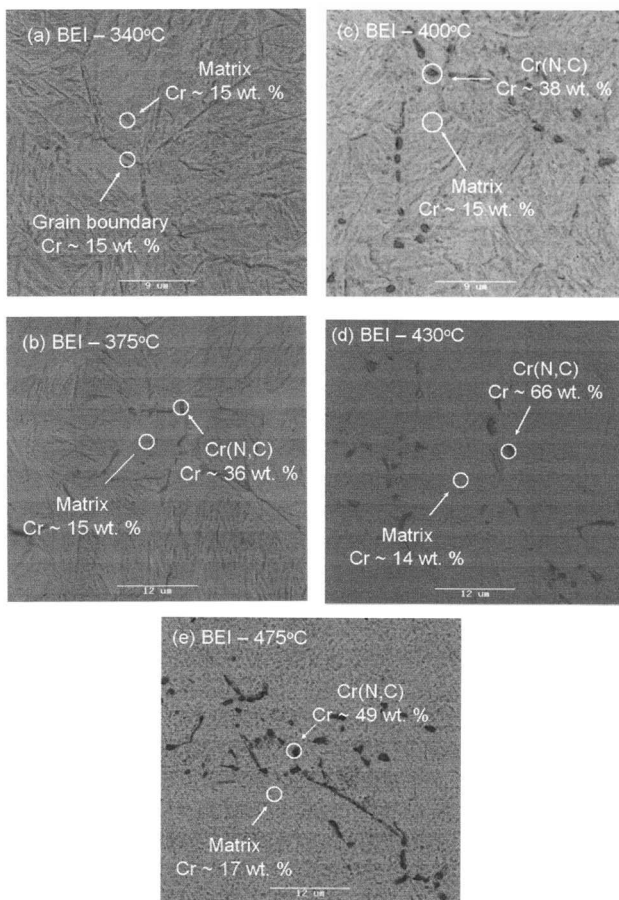
FIG. 6. [(a)–(e)] Evolution of backscattering electron images (BEI mode) of the surface of implanted samples as a function of temperature. The chromium content at grain boundaries and in matrix are indicated.
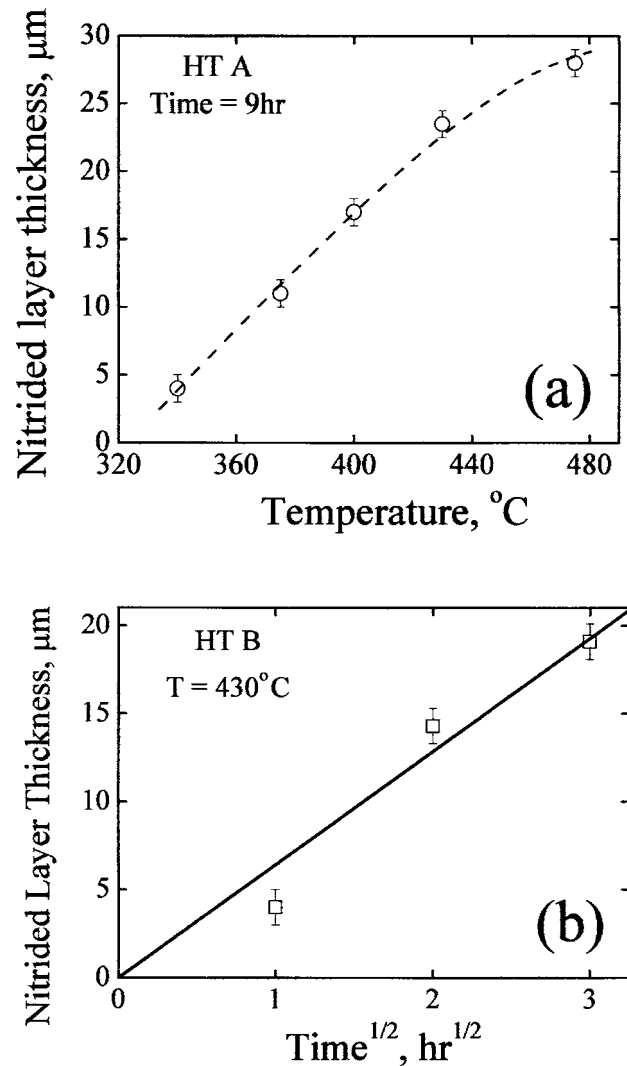

FIG. 7. [(a) and (b)] Evolution of the nitrided layer thickness as a function of implantation temperature (HT A samples and time process of 9 h) and the square root of the time process (HT B samples and temperature of 430 °C), respectively.

havior of the implanted samples with HT B has been described elsewhere, showing the same qualitative tendency.[24]

From cross-section analysis of the samples, the thickness of the nitrided layers can be obtained. Figure 7(a) shows the evolution of the nitrided layer thickness as a function of the implantation temperature and fixed time of 9 h using samples with HT A. The thickness increases linearly with temperature up to ~475 °C. Further temperature increments cause a generalized CrN precipitation, changing the previous process diffusion mechanism. Comparing these results to others where samples of austenitic stainless steels (ASS) AISI 316 were nitrided by PI³, the thickness of nitrided MSS is higher than that of nitrided ASS by 20%.[25] This faster diffusion of nitrogen can be explained by the crystalline structure, where nitrogen has a higher diffusion coefficient in bcc-like (MSS) versus fcc-like (ASS) structures.[26] Figure 7(b) shows the evolution of the nitrided layer thickness as the function of the square root of the implantation time at constant temperature (430 °C) for the HT B samples. It is clearly seen that the growth of the nitrided layer is in agreement with the parabolic law.[27]

The corrosion resistance of martensitic stainless steels depends on the proportion of chromium segregation from the matrix. Table III shows the breakdown potential of the im-

planted samples at 9 h with previous HT A and B. Bearing in mind that the corrosion properties are determined by the attacking medium, the presence of chloride ions probes the pitting corrosion, i.e., the possible penetration path of the aggressive ions.[28] Taking one of the series of samples, the more positive the breakdown potential, the better the pitting corrosion resistance. Figure 8 shows the evolution of the breakdown potential as a function of the implantation temperature using samples with HT A. The curve is a guide for the eyes and shows that temperatures from 375 to 400 °C are critical for abrupt segregations of chromium from the matrix. This degradation process of the corrosion resistance starts with precipitations of CrN (mostly) at the boundary grain at intermediate temperatures and becomes more important in all the grain (matrix) at higher temperatures [see Figs. 6(a)–6(e)].[29] On the other hand, Table III shows that the unimplanted sample treated with HT A has a better pitting corrosion resistance than samples with HT B. The lower tem-

TABLE III. Breakdown potentials obtained by potentiostatic anodic polarization in 3% NaCl of implanted samples in both HT at variable temperature and fixed process time of 9 h. The potential was corrected, taking the value of the reference electrode (235 mV). The unimplanted samples was added for comparison purposes.

Temperature (°C)	Breakdown potential (HT A) (mV)	Breakdown potential (HT B) (mV)
340	437	⋯
360	⋯	104
375	365	⋯
400	−29	⋯
430	−143	−132
475	−158	⋯
500	⋯	−245
Untreated	28	−200

pered temperature of the HT A induces less intergranular sensitization by a smaller quantity of precipitates of Cr_xC (chromium carbide) at grain boundary. Finally, the formation of a more compact structure, i.e., that of ε-$(Fe,Cr)_3N$ and/or γ_N-$(Fe,Cr)_4N$ phases, without any chromium segregation and lower tempered temperatures, improves the corrosion resistance of the original material.

IV. CONCLUSIONS

In conclusion, commercial martensitic stainless steel AISI 420 was nitrided by the PI^3 technique using two different previous heat treatments. At lower and intermediate implantation temperatures (from 340 to 430 °C), different phase transformations were obtained due to the initial proportion of retained austenite in the martensite structure. Apparently, there is a limited quantity of γ-austenite that induces fcc-like structures (γ and γ_N). At higher implantation temperatures, the great chromium mobility produced larger segregations of
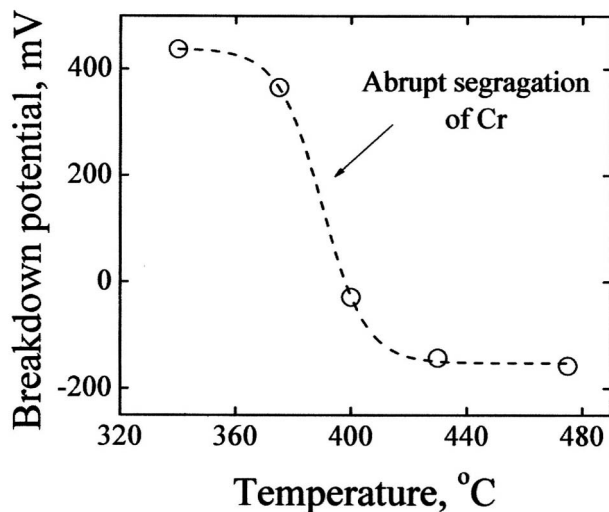

FIG. 8. Evolution of the breakdown potential as a function of the implantation temperature using samples with HT A and a process time of 9 h. The line is a guide for the eyes.

CrN with a random distribution and degraded the α'-martensite to α-Fe (ferrite). The nitrided layer thickness follows a fairly linear relationship with temperature and a parabolic law with time treatment. Moreover, the nitrided layer in MSS is 20% thicker than that in ASS in similar treatment conditions. The corrosion resistance depends on chromium segregation from the martensitic matrix due to the temperature of the implantation process (mostly precipitates of CrN) and the previous heat treatment (precipitates of CrC). Moreover, the process of heat treatment has become a parameter in plasma nitriding of metastable steels. Starting from the same base material, mechanical and chemical properties of the modified surface can be changed only with an accurate previous heat treatment. Finally, the best results are obtained using low tempering temperature and low implantation temperature (below 375°) due to the increment of the corrosion resistance and nitrogen dissolution in the structure with not too high diffusion depths (about $5-10$ μm).

[1]C. Blawert and B. L. Mordike, Surf. Coat. Technol. **93**, 274 (1997).
[2]Y. Sun and T. Bell, Wear **218**, 34 (1998).
[3]A. H. Deutchman, R. J. Partyka, and C. Lewis, in *Conference Proceedings of the ASM-Second International Conference, Cincinnati, Ohio, USA*, edited by T. Spalvins and W. L. Kovacs (ASM Int., Ohio, 1989), p. 29.
[4]M. J. Baldwin, G. A. Collins, M. P. Fewell, S. C. Haydon, S. Kumar, K. T. Short, and J. Tendys, Jpn. J. Appl. Phys., Part 1 **36**, 4941 (1997).
[5]R. W. K. Honeycombe, *Steel: Microstructure and Properties* (Edward Arnold, London, 1981).
[6]J. M. Priest, M. J. Baldwin, M. P. Fewell, S. C. Haydon, G. A. Collins, K. T. Short, and J. Tendys, Thin Solid Films **345**, 113 (1999).
[7]C. A. Figueroa, D. Wisnivesky, and F. Alvarez, J. Appl. Phys. **92**, 764 (2002).
[8]C. A. Figueroa, A. S. Ferlauto, and F. Alvarez, J. Appl. Phys. **94**, 5435 (2003).
[9]C. A. Figueroa and F. Alvarez, Surf. Coat. Technol. **200**, 398 (2005).
[10]G. A. Collins, R. Hutchings, K. T. Short, and J. Tendys, Heat Treat. Met. **4**, 91 (1995).
[11]J. R. Conrad, J. L. Radtke, R. A. Dodd, F. J. Worzala, and N. C. Tran, J. Appl. Phys. **62**, 4591 (1987).
[12]S. Mandl, R. Gunzel, E. Richter, and W. Moller, Surf. Coat. Technol. **101**, 372 (1998).
[13]M. Ueda, L. A. Berni, J. O. Rossi, J. J. Barroso, G. F. Gomes, A. F. Beloto, and E. Abramof, Surf. Coat. Technol. **136**, 28 (2001).
[14]M. P. Fewell, J. M. Priest, M. J. Baldwin, G. A. Collins, and K. T. Short, Surf. Coat. Technol. **131**, 284 (2000).
[15]G. A. Collins, R. Hutchings, K. T. Short, and J. Tendys, Surf. Coat. Technol. **103/104**, 212 (1998).
[16]C. Blawert, B. L. Mordike, G. A. Collins, K. T. Short, and J. Tendys, Surf. Coat. Technol. **104**, 240 (1998).
[17]Z. Yu, X. Xu, L. Wang, J. Qiang, and Z. Hei, Surf. Coat. Technol. **153**, 125 (2002).
[18]S. K. Kim, J. S. Yoo, J. M. Priest, and M. P. Fewell, Surf. Coat. Technol. **163/164**, 380 (2003).
[19]A. Muñoz-Páez, J. I. F. Peruchena, J. P. Espinós, A. Justo, F. Castañeda,

S. Días-Moreno, and D. T. Bowron, Chem. Mater. **14**, 3220 (2002).

[20]L. Reimer, *Scanning Electron Microscopy: Physics of Image Formation and Microanalysis* (Springer, Berlin, 1985).

[21]A. Toro, W. Z. Misiolek, and A. P. Tschiptschin, Acta Mater. **51**, 3363 (2003).

[22]*Proceedings of a Symposium Sponsored by the TMS-AIME Heat Treatment Committee at the TMS Fall Meeting, Niagara Falls, New York, USA*, edited by K. C. Russell and H. I. Aaronson (The Metallurgical Society of AIME, 1976), p. 137.

[23]P. E. F. Flewitt and R. K. Wild, *Grain Boundaries: Their Microstructure and Chemistry* (Wiley, Chichester, 2001).

[24]C. A. Figueroa, F. Alvarez, Z. Zhang, G. A. Collins, and K. T. Short, J. Vac. Sci. Technol. A **23**, 693 (2005).

[25]G. A. Collins, R. Hutchings, K. T. Short, J. Tendys, X. Li, and M. Samandi, Surf. Coat. Technol. **74/75**, 417 (1995).

[26]J. S. Kirkaldy and D. J. Young, *Diffusion in the Condensed State* (The Institute of Metals, London, 1987).

[27]V. I. Dimitrov, J. D'Haan, G. Knuyt, C. Quasyhaegens, and L. M. Stals, Appl. Phys. A: Mater. Sci. Process. **63**, 475 (1996).

[28]C. Blawert, H. Kalvelage, B. L. Mordike, G. A. Collins, K. T. Short, Y. Jirásková, and O. Schneeweiss, Surf. Coat. Technol. **136**, 181 (2001).

[29]M. Samandi, B. A. Shedden, D. I. Smith, G. A. Collins, R. Hutchins, and S. Tendys, Surf. Coat. Technol. **59**, 261 (1993).